



# 1 **Inversion of Residual Gravity Anomalies using Tuned-PSO** 2 **Technique**

3 Ravi Roshan and Upendra Kumar Singh

4 Department of Applied Geophysics, Indian School of Mines, Dhanbad – 826 004, India

5 Correspondence: [roshanravi.sinha@gmail.com](mailto:roshanravi.sinha@gmail.com)

## 6 **Abstract**

7 Many kinds of particle swarm optimization (PSO) technique are now available and various  
8 efforts have been made to solve linear and non linear problems as well as one dimensional  
9 and multidimensional problem of geophysical data. Particle swarm optimization is a Meta  
10 heuristic optimization method that requires the intelligent guess and suitable selection of  
11 controlling parameters (i.e. Inertia weight and acceleration coefficient) for better convergence  
12 at global minima. The proposed technique Tuned-PSO is an improved technique of PSO, in  
13 which effort has been made for choosing the controlling parameters and these parameters  
14 have selected after analysing the response of various possible exercises using synthetic  
15 gravity anomalies over various geological sources. The applicability and efficacy of the  
16 proposed method is tested and also validated using synthetic gravity anomalies over various  
17 source geometries. Finally Tuned-PSO is applied over field residual gravity anomalies of two  
18 different geological terrains to find out the model parameters namely amplitude coefficient  
19 factor ( $A$ ), shape factor ( $q$ ) and depth ( $z$ ). The analysed results have been compared with  
20 published results obtained by different methods that show a significantly excellent agreement  
21 with real model parameters. The results also show that the proposed approach is not only  
22 superior to the other methods but also shows that the strategy has enhanced the exploration  
23 capability of proposed method. Thus Tuned-PSO is an efficient and more robust technique to  
24 achieve optimal solution with minimal error.

25 *Keywords: Tuned-PSO, gravity anomalies, inversion.*

## 27 **1. Introduction**

28 Gravity method is based on the measurement of gravity anomalies caused by the density  
29 variation due to source anomalies. Gravity method has been used in a wide range of  
30 application as a reconnaissance method for oil exploration and as a secondary method for  
31 mineral exploration, to find out the approximate geometry of the source anomalies, bedrock  
32 depths, and shapes of the earth. Interpretation of geophysical data that involves solving an



33 inverse problem; many techniques have been developed to invert the geophysical data to  
34 estimate the model parameters. These methods can be broadly categorised into two groups:  
35 (1) local search technique ( e.g. Steepest descent method; conjugate gradient method, ridge  
36 regression, Levenberg- Marquardt method etc.) and (2) global search techniques (e.g.,  
37 simulated annealing, genetic algorithms, particle swarm optimization, Ant colony  
38 optimization etc.) Local search technique is simple and requires a very good initial  
39 presumption – close to true model for a successful convergence. In other hand global search  
40 method may provide an acceptable solution but computationally time intensive. There are  
41 several local and global inversion technique has been developed to interpret gravity  
42 anomalies (Thanassoulas *et al.*, 1987; Shamsipour *et al.*, 2012; Montesinos *et al.*, 2005; Qiu,  
43 2009; Touthmalani, 2013). However, PSO has been successfully applied in many fields, such  
44 as model construction, biomedical images, electromagnetic optimization, hydrological  
45 problem etc. (Cedeno and Agrafiotis, 2003; Wachowiak *et al.*, 2004; Boeringer and Werner,  
46 2004; Kumar and Reddy, 2007; Eberhart and Shi, 2001; El-Kaliouby and Al-Garni, 2009) but  
47 in the geophysical field PSO has limited number of applications (Alvarez *et al.*, 2006; Shaw  
48 and Srivastava, 2007).

49 In this paper improved Particle Swarm Optimization known as Tuned-PSO with fine  
50 tuning of learning parameters have been tested using synthetic gravity anomalies over kinds  
51 of geometrical bodies and compared their efficacy. On the basis of performance, finally  
52 Tuned PSO has been used to invert gravity anomalies to find out the essential model  
53 parameters such as shape factor (q), depth (z), amplitude coefficient factor (A) and horizontal  
54 location of the source geometry.

## 55 **2. Forward modelling for generating the synthetic gravity anomalies**

56 A general expression of gravity anomaly caused by a sphere, an infinite long horizontal  
57 cylinder and a semi-infinite vertical cylinder have been used for generating the gravity  
58 anomalies in forward problem that is given in equation 1 (Abdelrahman *et al.*, 1989) as  
59 follows:

$$60 \quad g(x_i, z, q) = A \frac{z^m}{(x_i^2 + z^2)^q} \quad (1)$$

61 Where

$$62 \quad A = \begin{cases} \frac{4}{3} \pi G \sigma R^3 & \text{for a sphere ,} \\ 2 \pi G \sigma R^2 & \text{for a horizontal cylinder,} \\ \pi G \sigma R^2 & \text{for a vertical cylinder,} \end{cases} \quad m = \begin{cases} 1, \\ 1, \\ 0, \end{cases}$$



$$q = \begin{cases} \frac{3}{2} & \text{for sphere,} \\ 1 & \text{for horizontal cylinder,} \\ \frac{1}{2} & \text{for a vertical cylinder ; } R \ll Z. \end{cases}$$

Where A, q and z represent amplitude coefficient factor, shape factor and depth respectively; and  $x_i$ ,  $\sigma$ , G and R are the position coordinate, density contrast, universal gravitational constant and radius of geometrical bodies respectively. For semi-infinite vertical cylinder the gravity response is only applicable when the radius of the cylinder is much smaller than the distance from observation position to the top of the cylinder. In the forward modelling for generating the synthetic gravity anomalies, the amplitude coefficient factor of 600 mGal\*km<sup>2</sup> and 200 mGal for sphere and vertical cylinder respectively, correspond to the shape factor as 1.5 and 0.5, and the depth of 5.0 km and 3.0 km are used. The shape factor approaches to zero as the structure becomes a nearly horizontal bed and approaches 1.5 as the structure becomes a perfect sphere (point mass). As in the formulae  $x_i$  is the position coordinate; at the origin  $x_i = 0$  then equation 1 becomes,

$$g(0) = \frac{A}{z^{2q-m}} \quad (2)$$

The equation 3 is taken for addition of 10% white Gaussian noise.

$$g_{noisy}(x) = awgn(g(x), 0.1) \quad (3)$$

### 3. Tuned- Particle Swarm Optimization (Tuned-PSO)

Tuned-Particle Swarm Optimization (Tuned-PSO) is an improved Particle swarm optimization (PSO) method after the fine tuning of its learning parameters. The concept of PSO is described as follows (Eberhart and Kennedy, 1995): (a) each potential solution called as particles and knows its best values so far ( $P_{best}$ ) and its position more over each particle knows the best value in the group ( $G_{best}$ ) among the  $P_{best}$ . All of the best values are based on objective function ( $Q$ ) for each problem to be solved. Each particle tries to modify its position through the current velocity and its positions. The velocity of each particle can be updated using the following equations (Santos, 2010):

$$\begin{aligned} v_i^{k+1} &= \omega^k v_i^k + c_1 rand() * (P_{best-i}^k - x_i^{k+1}) + c_2 rand() * (G_{best}^k - x_i^{k+1}) \\ x_i^{k+1} &= x_i^k + v_i^{k+1} \end{aligned} \quad (4)$$



96 Where  $v_i^k$  is the velocity of  $i_{th}$  particle at  $k_{th}$  iteration,  $x_i^k$  represents current position of  $i_{th}$   
97 particle at  $k_{th}$  iteration,  $rand()$  is a random number in the range of 0 and 1.  $c_1$  &  $c_2$  are  
98 constants known as cognitive coefficient and social coefficient respectively. The coefficient  
99  $c_1$  has contribution towards the self exploration of a particle and the coefficient  $c_2$  has a  
100 contribution towards the motion of the particles in global direction, and  $\omega$  is an inertia  
101 weight in the range [0, 1]. The objective function has calculated by following equation  
102 (Santos, 2010).

$$103 \quad Q = \frac{2 \sum_i^N |v_i^o - v_i^c|}{\sum_i^N |v_i^o - v_i^c| + \sum_i^N |v_i^o + v_i^c|} \quad (5)$$

104 Where N is the number of iteration,  $v_i^o$  and  $v_i^c$  are observed and calculated gravity anomaly  
105 measured at point  $p(x_i)$  respectively.

106

## 107 **4 Discussion and Results**

### 108 **4.1 Selection of learning parameter for Tuned-PSO Modelling**

109 In this paper, a judicious selection of the parameters (i.e.  $\omega$ ,  $c_1$ , and  $c_2$ ,) has been discussed  
110 for controlling the convergence behaviours of Tuned-PSO based algorithm. The settings of  
111 these parameters determine how it optimizes the search-space. These algorithms with suitable  
112 selection of parameter become more powerful global search algorithm for their practical  
113 applications.

#### 114 **4.1.1 Inertia weight**

115 Inertia weight  $\omega$  controls the momentum of the particle (Eberhart and Shi, 2001; Eberhart and  
116 Kennedy, 1995). Here two kinds of source geometry are adopted to evaluate more suitable  
117 ranges of parameters in the Tuned-PSO. For tuning of inertia weight, 0, 0.4, 0.7, 0.9, has been  
118 taken for two different acceleration coefficients at 1.4 and 2.0 respectively. From Figure 1, it  
119 is clear that the best convergence has performed by algorithm at inertia weight 0.7. This value  
120 of inertia weight produces high convergence rate at less number of iteration than the other  
121 values.

#### 122 **4.1.2 The maximum velocity $v_{max}$**

123 The maximum velocity  $v_{max}$  determines the maximum change one particle can undergo in its  
124 positional coordinates during iteration and used to avoid explosion and divergence. Usually,  
125 the full search ranges of the particle's positions as the  $v_{max}$  are fixed. For example, in case,  
126 a particle has position vector  $x = (x_1, x_2, x_3)$  and if  $-15 \leq x_i \leq 15$  for  $i=1, 2$  and  $3$ , then  $v_{max} =$   
127  $30$  is fixed.



128

#### 129 **4.1.3 The swarm size**

130 It is quite a common practice in the PSO literature to limit the range of number of particles.  
131 Van den Bergh and Engelbrecht have shown that though there is a slight improvement of the  
132 optimal value with increasing swarm size, a larger swarm increases the number of function  
133 evaluations to converge to an error limit. However, Eberhart and Shi Illustrated that the  
134 population size has hardly any effect on the performance of the PSO method. So, in this paper  
135 population size has taken 100.

136

#### 137 **4.1.4 The acceleration coefficients $c_1$ and $c_2$**

138 To find the best tuning of learning parameters, various values of  $c_1$ ,  $c_2$  (i.e.  $c_1 = c_2 = 1.0, 1.2,$   
139  $1.4, 1.6, 1.8,$  and  $2.0$ ) and inertia weights (i.e.  $0.4, 0.7$  and  $0.9$ ) are taken, and various  
140 exercises have been made using the two different geometrical bodies by fixing the each of the  
141 inertia weight (Table 1). The results was analysed and found that more suitable values of  $c_1$   
142 and  $c_2$  (i.e.  $c_1 = c_2 = 1.4$ ) are the best tuned acceleration coefficients for our case. These  
143 values of acceleration coefficients have been used to invert the gravity anomalies, which  
144 provide significant improvement and produce optimal solutions of the geological bodies.

145

#### 146 **4.2 Application to Synthetic gravity anomalies**

147 Initially two geometrical models i.e. sphere and vertical cylinder has been considered for  
148 testing the applicability and efficacy of Tuned-PSO. The efficacy of proposed algorithm in  
149 terms of RMS error versus iterations is as shown in Figure 1. The gravity anomalies over  
150 these models are computed from equation (1) for the model parameters as shown in Table  
151 1(a, b) and 2(a, b). In each case, the length of gravity profile of 51 km has 51 data points at  
152 one km equal interval. The gravity anomaly for every source model is corrupted with 10% of  
153 white gaussian noise and Tuned-PSO based inversion algorithms applied on them. The  
154 optimized results obtained by Tuned-PSO algorithms for synthetic noise free and with 10%  
155 noisy data. The Figure 1 shows that tuned-PSO has best results at values 1.4, 1.4 and 0.7 for  
156  $c_1$ ,  $c_2$  and inertia weight ( $w$ ) respectively. This also shows that Tuned-PSO curve is having  
157 less number of local minima than other values. It means that the Tuned-PSO technique  
158 minimise the number of local minima for solving the geophysical nonlinear inverse problems.  
159 The simulated gravity anomaly by Tuned-PSO and computed gravity anomaly are shown in  
160 Figure 2(a) and 3(a) respectively and correspond to synthetic gravity anomaly and computed  
161 anomaly corrupted with 10% of white gaussian noise as shown in Figure 2(b) and 3(b).



162 Figure 2 and Figure 3 show the well matching between the synthetic curves and Tuned-PSO  
163 calculated gravity anomalies curves over spherical model and vertical cylindrical model  
164 respectively. Figure 4 shows the behaviour of  $p_{best}$  and  $g_{best}$  variation inside the algorithm and  
165 suggests that  $g_{best}$  decreases more rapidly toward the minimal error with high convergence.  
166 We observed from Table 2 and 3 that the RMS error increases with increasing the noise in  
167 gravity anomaly however, the horizontal location ( $x_0$ ) is a substantially stable parameter and  
168 varies in a small scale.

169

#### 170 **4.3 Application to Field gravity anomalies**

##### 171 **4.3.1. Moberun Sulphide Body, Near Rouyn- Noranda, Canada**

172 Moberun polymetallic deposit near Rouyn- Noranda comprises two complexes of massive  
173 lenses within mainly felsic volcanic rocks of the Archean Blake River Group (Barrett. *et al.*,  
174 1992). The main lens contents mainly massive sulphide, approximately 3.37 Million Ton  
175 with some other elements in least amount in comparison to sulphide are 0.95 Million Ton at  
176 0.81% Cu, 2.44% Zn, 30.3 g/t Ag, and 2.2 g/t Au estimated in 1989. The 1100 complex is  
177 located at 250 m to southeast of the Main complex. Host volcanic rocks of main complex are  
178 mostly massive, brecciated, and tuffaceous rhyolites. Moberun ore body is located at shallow  
179 depth; top of the body approximately 30 m depth and extended to 175 m.

180 Tuned-PSO in MATLAB environment has been applied to field residual gravity  
181 anomaly. This anomaly profile of length 268 m has been taken from the Moberun sulphide  
182 body, Noranda, Canada (Nettleton, 1976; Essa, 2012). It is seen from Figure 5 that both  
183 curves analysed from Tuned-PSO and observed gravity anomalies are extremely well  
184 correlated with optimal RMS error of 0.0271%. The results in terms of model parameters  
185 (amplitude coefficient factor, shape factor and depth) over the Moberun ore body analysed  
186 from Tuned-PSO method can be seen in Table 4(a). This table provides the optimum results  
187 obtained from Tuned-PSO with 0.0271% error agrees well with the results obtained from  
188 other methods. The calculated value of shape factor,  $q$  is 0.77 (Table 4a). This value over  
189 Moberun sulphide ore body reflects the shape of a semi-infinite vertical cylindrical geological  
190 body is present at depth of 30 m. It can be seen from Table (b), the values of amplitude  
191 coefficient factor, shape factor and depth correspond to 60.0, 0.77 and 30 are more stable and  
192 consistent with results analysed from various authors.

193

194

195



196 **4.3.2. Louga Anomaly West coast of Senegal, West Africa**

197 The study area Louga anomaly of west coast of Senegal is taken for another case study for  
198 interpretation of gravity data using Tuned –PSO. The Senegal basin is part of the north-west  
199 African coastal basin- a typical passive margin basin opening west to the Atlantic. The  
200 complexities of the rift tectonics of the Atlantic opening gave rise to a series of sub-basins  
201 aligned north-south. The pre-rift (Upper Proterozoic to Palaeozoic), syn-rift (Permian to  
202 Lower Jurassic) and post-rift are divided into a number of sub-basins, controlled by east west  
203 transform related lineaments (Nettleton, 1962). In this paper Tuned-PSO in MATLAB  
204 environment has been also applied to another field case study. Gravity anomaly of Louga  
205 area, West coast of Senegal, West Africa (Essa, 2014) has taken for Tuned- PSO analysis as  
206 shown in Figure 6 has Profile length 32 km. The results in terms of model parameters  
207 (amplitude coefficient factor, shape factor and depth) over the Louga anomaly analysed from  
208 Tuned-PSO method can seen in Table 5(a). It is seen from Figure 6 that both curves analysed  
209 from Tuned-PSO and observed gravity anomalies are extremely well correlated with optimal  
210 RMS error of 0.0271%. The optimum obtained results of model parameters amplitude  
211 coefficient factor (A), shape factor (q) and depth (z) are 545.30 mGal, 0.53 and 4.92 km  
212 respectively that shows significantly good agreement with the results obtained by various  
213 authors as shown in Table 5(b). The Tuned PSO analysed value of shape factor confirms that  
214 the shape of the causative body is semi-infinite vertical cylindrical body present at depth  
215 about 4.92 km.

216

217 **5. Conclusions**

218 In this paper, various synthetic gravity anomalies and field gravity anomalies have been  
219 adopted for evaluating the applicability and efficacy of Tuned-PSO algorithms and also  
220 determining the suitable ranges of learning parameters setting (i.e. inertia weight and  
221 acceleration coefficients). On the basis of the performance, a novel algorithm PSO with  
222 suitable learning parameters has been implemented to gravity anomalies assuming models  
223 with gravity source geometry such as sphere and vertical cylinder. This technique has been  
224 tested and demonstrated on synthetic gravity anomalies with and without gaussian noise and  
225 finally applied to field residual gravity anomalies over Mobrun sulphide ore body, Noranda,  
226 QC, Canada and Louga Anomaly of West coast of Senegal, West Africa. This technique  
227 provides robust and plausible results even in the presence of noise that are consistent with the  
228 results obtained from other classical methods. Thus this technique is powerful tool that



229 improves the results of classical PSO and other technique significantly with less time and  
230 optimal error.

231

232

## 233 6. References

234 Abdelrahman, E.M., Bayoumi, A.I., Abdelhady, Y.E., Gobashy, M.M., El-Araby, H.M.,  
235 1989. Gravity interpretation using correlation factors between successive least-  
236 squares residual anomalies. *Geophysics*, 54, 1614-1621.

237 Alvarez, J.P.F., Marti`nez, F., Gonzalo, E.G., Pe`rez, C.O.M., 2006. Application of the  
238 particle swarm optimization algorithm to the solution and appraisal of the vertical  
239 electrical sounding inverse problem. In: proceedings of the 11<sup>th</sup> Annual Conference of  
240 the international Association of Mathematical Geology (IAMG06), Li\_ege, Belgium,  
241 CDROM.

242 Barrett, T.J., Cattalani, S., Holy, L., Riopel, J., Lafleur, P.J., 1992. Massive sulphide deposits  
243 of the Noranda area, Quebec .IV. The Mobrun mine. *Canadian Journal of Earth  
244 Science*, 29(7), 1349-1374, 10.1139/e92-110.

245 Boeringer, D.W., Werner, D.H., 2004. Particle swarm optimization versus genetic algorithms  
246 for phased array synthesis. *IEEE Transactions on Antennas and Propagation*, 52, 771–  
247 779.

248 Cedeno, W., Agrafiotis, D.K., 2003. Using particle swarms for the development of QSAR  
249 models based on K-nearest neighbour and kernel regression. *Journal of Computer  
250 Aided Molecular Design*, 17, 255–263.

251 Eberhart, R.C., Kennedy, J., 1995. A new optimizer using particle swarm theory. In:  
252 proceedings of the IEEE The sixth Symposium on Micro Machine and Human Centre,  
253 Nagoya, Japan, 39-43.

254 Eberhart, R.C., Shi, Y., 2001. Particle swarm optimization: developments, applications and  
255 resources. In: Proceedings of the Congress on Evolutionary Computation, Seoul,  
256 Korea, 81–86.

257 El-Kaliouby, H.M., Al-Garni, M.A., 2009. Inversion of self-potential anomalies caused by  
258 2D inclined sheets using neural networks. *Journal of Geophysics and Engineering*, 6,  
259 29–34. doi:10.1088/1742-2132/6/1/003.

260 Essa, K. S., 2007. Gravity data interpretation using s-curves method. *Journal of Geophysical  
261 Engineering*, 4, 204–13.





- 262 Essa, K.S., 2012. A fast interpretation method for inverse modelling or residual gravity  
263 anomalies caused by simple geometry. *Journal of Geophysical research*, Article ID  
264 327037, 10 pages.doi:10.1155/2012/327037.
- 265 Essa, K.S., 2014. New fast least squares algorithm for estimating the best fitting parameters  
266 dut to simple geometric structures from gravity anomalies. *Journal of Advanced*  
267 *research*, 5, 57-67.
- 268 Montesinos, F.G., Arnosó, j., Vieira, R., 2005. Using a genetic algorithm for 3-D inversion  
269 of gravity data in Fuerteventura (Canary Island). *International Journal of Earth*  
270 *Sciences (Geol Rundsch)*, 94, 301-316.
- 271 Nettleton, L.L., 1976. *Gravity and magnetic in oil prospecting*. New York: McGraw-Hill  
272 Book Co., 480.
- 273 Nettleton, LL. Gravity and magnetics for geologists and seismologists. *AAPG Bull* 1962, 46,  
274 1815–38.  
275
- 276 Qiu, N., Liu, Q., Gao, Q., 2009. Gravity Data inversion based genetic algorithm and  
277 Generalized least square. 978-1-4244-4738-1/09/\$25.00 ©2009 IEEE
- 278 Roy, L., Agarwal, B.N.P., Shaw, R.K., 2000. A new concept in Euler deconvolution of  
279 isolated gravity anomalies. *Geophysical prospecting*, 48, 3, 559-575.
- 280 Santos, F.A.M., 2010. Inversion of self – potential of idealized bodies’ anomalies using  
281 particle swarm optimization. *Computers and Geosciences*, 36, 1185-1190.
- 282 Shamsipour, P., Marcotte, D., Chouteau, M., 2012. 3D stochastic Joint Inversion of gravity  
283 and magnetic data. *Journal of Applied Geophysics*, 79, 27-37.
- 284 Shaw, R., Srivastava, S., 2007. Particle swarm optimization: a new tool to invert geophysical  
285 data. *Geophysics*, 72(2), 75-83.
- 286 Thanassoulas, C., Tselentis, G.-A., Dimitriadis, K., 1987. Gravity inversion of a fault by  
287 Marquardt’s Method. *Computer and Geosciences*, 13, 399-404.
- 288 Touthmalani, R., 2013. Comparision result of inversion of gravity data of a fault by particle  
289 swarm optimization and Levenberg-Marquardt methods. *SpringerPlus*, 2, 462.
- 290 Wachowiak, M.P., Smoli`kova`, R., Zheng, Y., Zurada, J.M., Elmaghraby, A.S., 2004. An  
291 approach to multimodal biomedical image registration utilizing particle swarm  
292 optimization. *IEEE Transaction on Evolutionary Computation*, 8(3), 289-301.  
293  
294  
295



296 **Figure and Table Captions**

297 Figure 1. Iteration versus RMS error plot at different acceleration coefficients and inertia  
298 weights.

299 Figure 2. (a) Synthetic gravity anomaly versus Tuned-PSO calculated gravity anomaly over  
300 spherical model and (b) Synthetic gravity anomaly versus Tuned-PSO calculated  
301 gravity anomaly over same model with 10% white gaussian noise.

302 Figure 3. (a) Synthetic gravity anomaly versus Tuned-PSO calculated gravity anomaly over  
303 vertical cylindrical model, (b) Synthetic gravity anomaly versus Tuned-PSO  
304 calculated gravity anomaly over same model with 10% white gaussian noise.

305 Figure 4. Iteration versus RMS error of Tuned-PSO showing  $p_{best}$  and  $g_{best}$  over synthetic  
306 gravity anomaly.

307 Figure 5. Observed field gravity anomaly versus Tuned-PSO calculated gravity anomaly over  
308 Moberun sulphide ore body, Canada.

309 Figure 6. Observed field gravity anomaly versus Tuned-PSO calculated gravity anomaly over  
310 West Senegal anomaly, Louga area, South Africa.

311 Table 1. Performance of the acceleration coefficients  $c_1$  and  $c_2$  using the synthetic gravity  
312 anomalies over spherical and vertical cylindrical geometrical bodies.

313 Table 2. (a) Optimized model parameters, converged iteration and RMS error in the inversion  
314 of synthetic gravity anomaly over a spherical source model and (b) optimized  
315 parameters, converged iteration and RMS error in the inversion of synthetic gravity  
316 anomaly with 10% white gaussian noise over a same source model from Tuned-PSO.

317 Table 3. (a) Optimized model parameters, converged iteration and RMS error in the inversion  
318 of synthetic gravity anomaly over a vertical cylindrical source model and (b)  
319 optimized parameters, converged iteration and RMS error in the inversion of synthetic  
320 gravity anomaly with 10% white gaussian noise over a same source model from  
321 Tuned-PSO.

322 Table 4. (a) Analysed results and parameters (A, z and q) used to invert the gravity anomaly  
323 over Moberun sulphide ore body and (b) comparative results over Moberun field,  
324 Canada from various methods and Tuned- PSO.

325 Table 5. (a) Analysed results and parameters (A, z and q) used to invert the gravity anomaly  
326 over West Senegal anomaly, Louga area, South Africa and (b) comparative results  
327 over same area from various methods and Tuned- PSO.

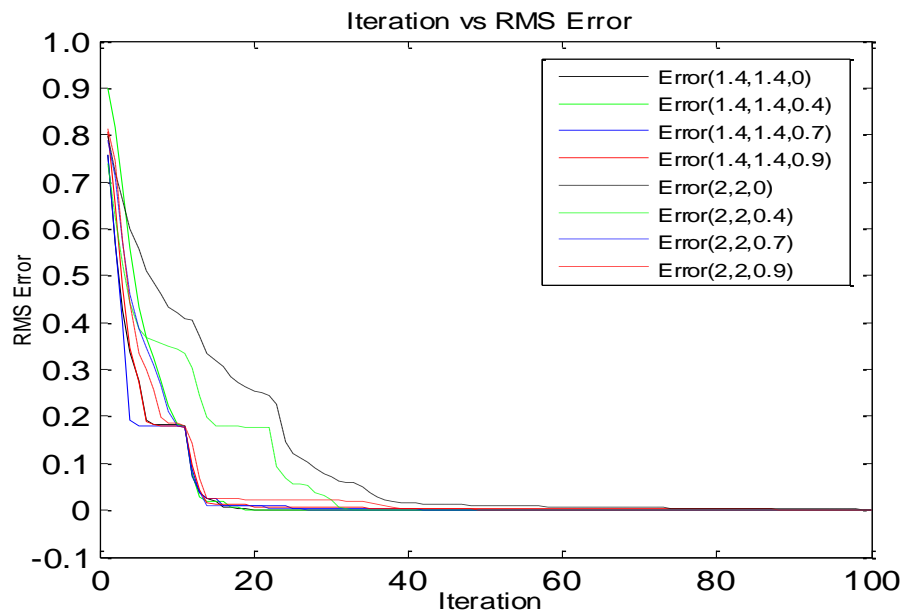
328

329



330  
331

Figure 1

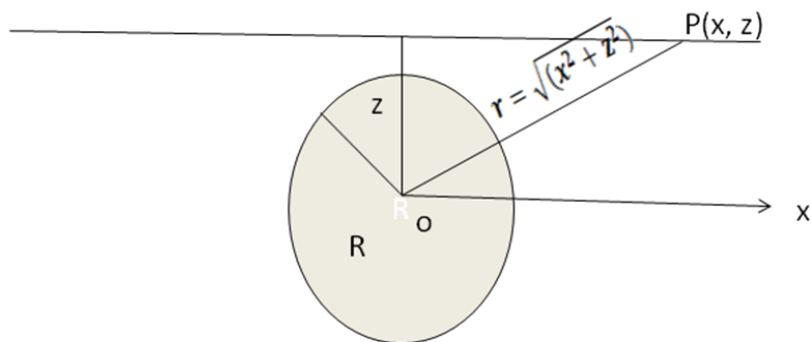
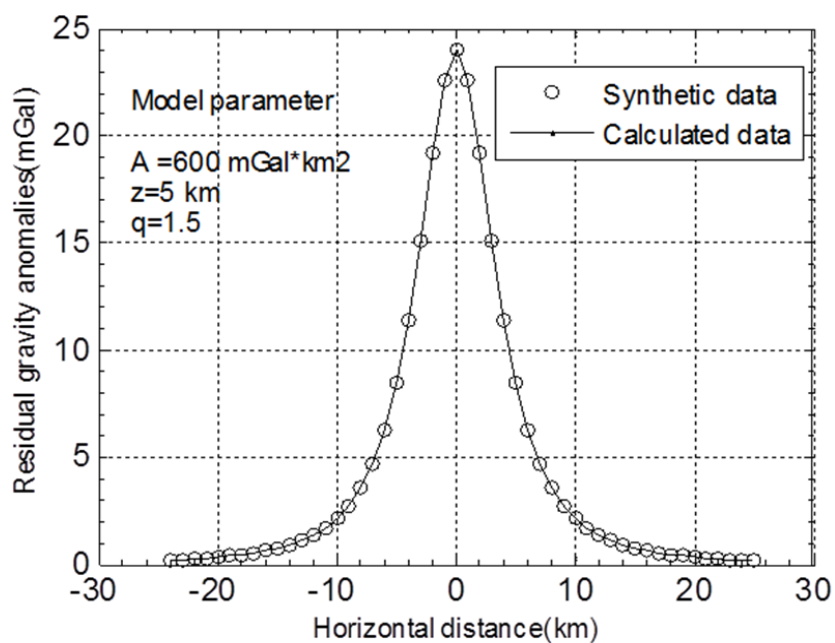


332  
333



334  
 335  
 336

Figure 2(a)

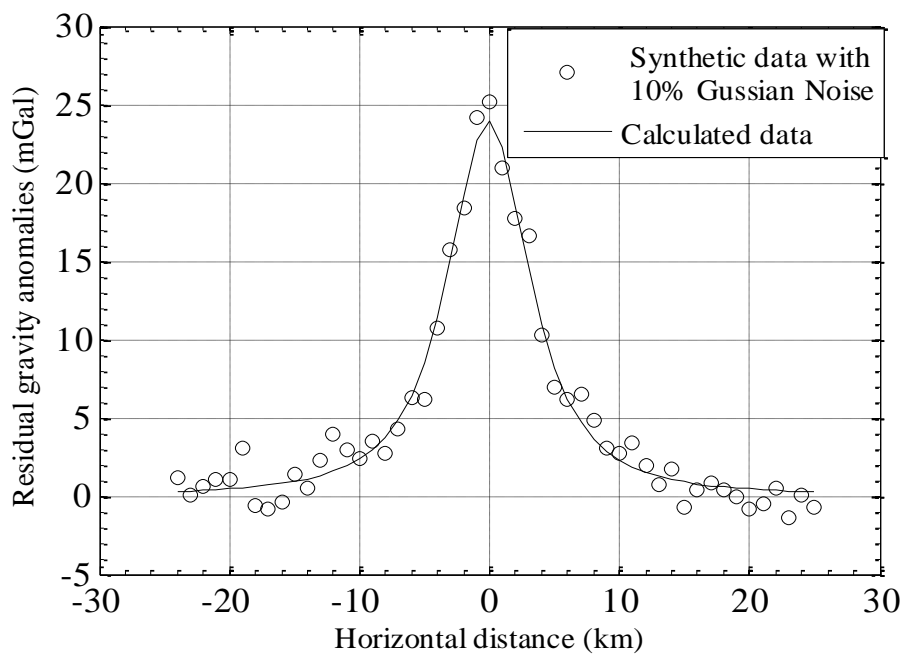


337  
 338  
 339  
 340  
 341  
 342  
 343  
 344



345  
346  
347

Figure 2(b)

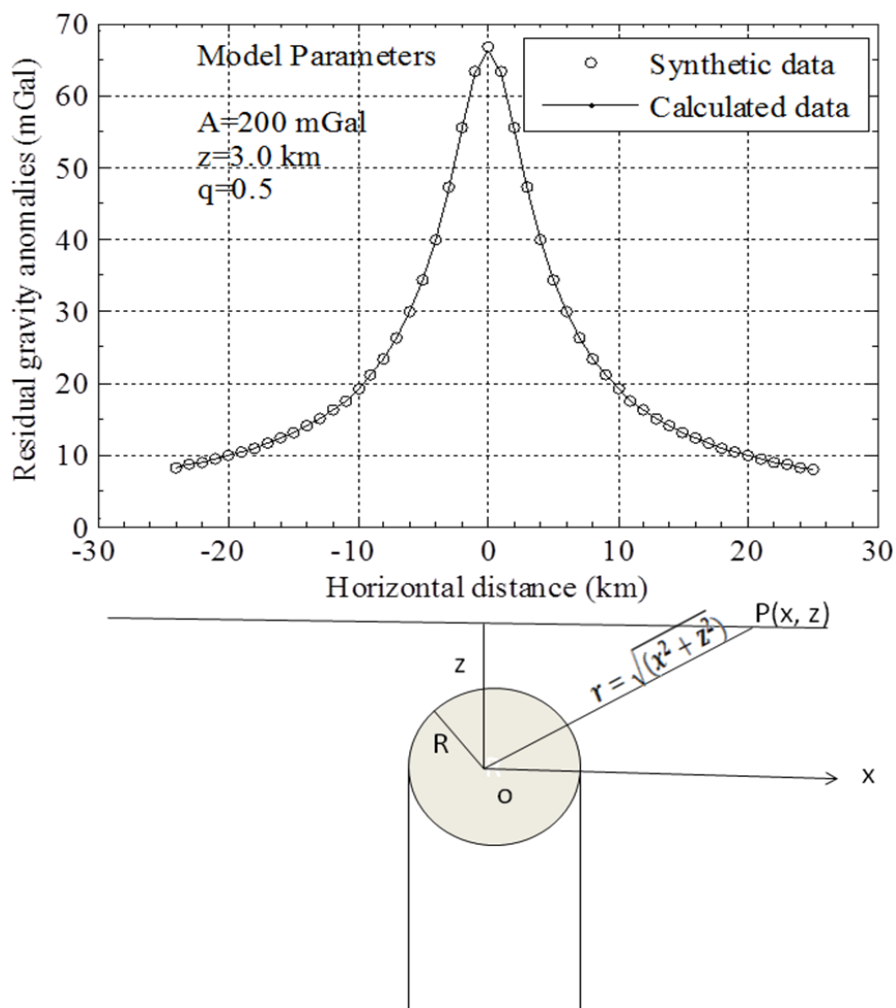


348  
349  
350  
351  
352  
353



354  
 355  
 356

Figure 3(a)

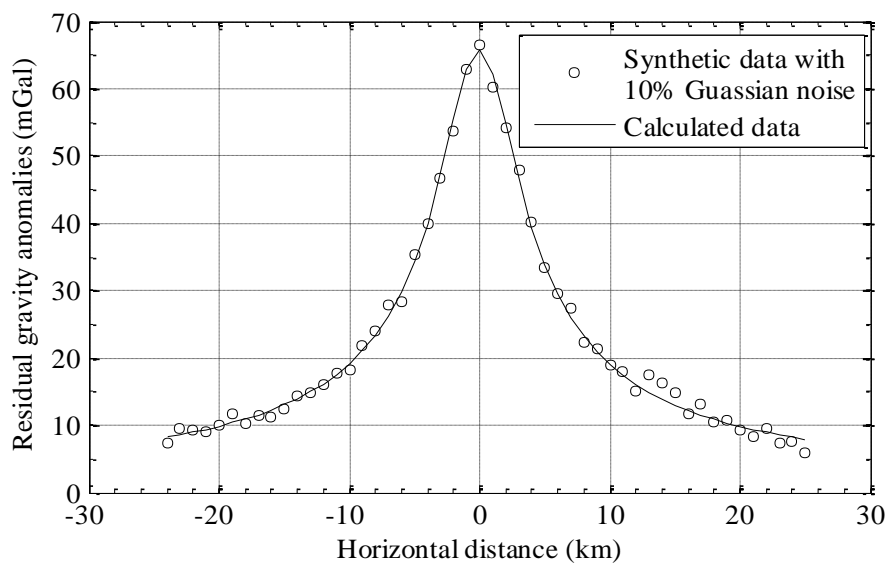


357  
 358  
 359  
 360  
 361  
 362  
 363  
 364



365  
366  
367

Figure 3(b)

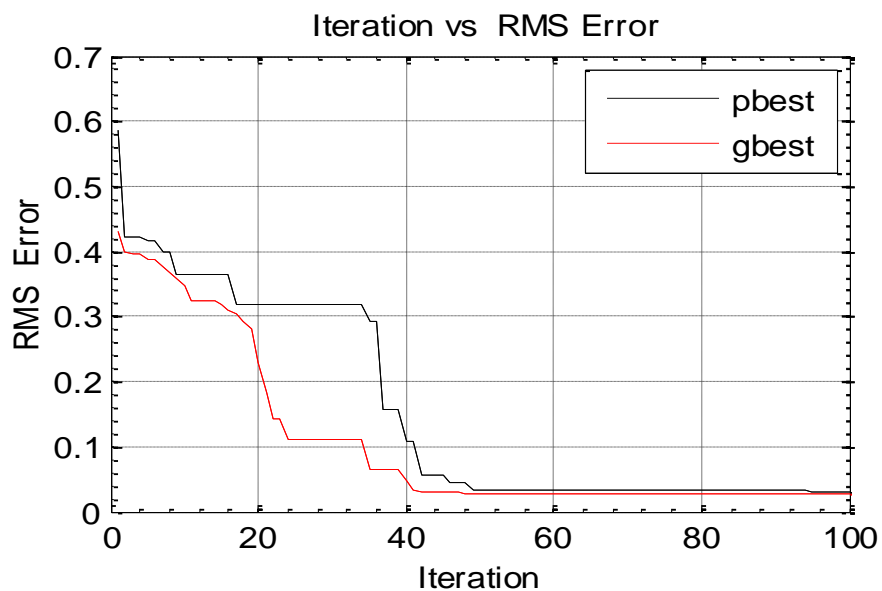


368  
369  
370  
371  
372  
373  
374  
375  
376  
377  
378  
379  
380  
381  
382  
383  
384  
385  
386



387  
388  
389

Figure 4



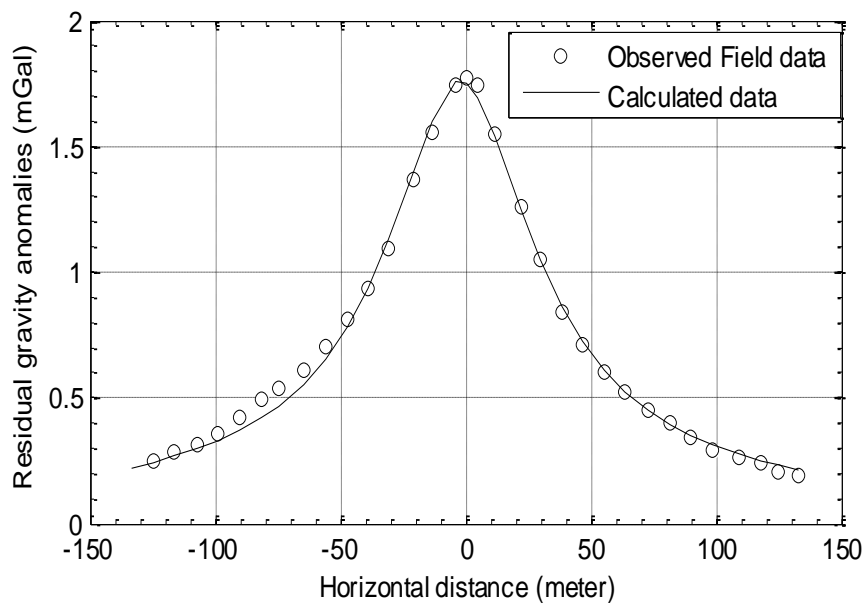
390  
391  
392  
393  
394  
395  
396  
397  
398  
399  
400  
401  
402  
403  
404  
405  
406  
407  
408





409  
410  
411

Figure 5

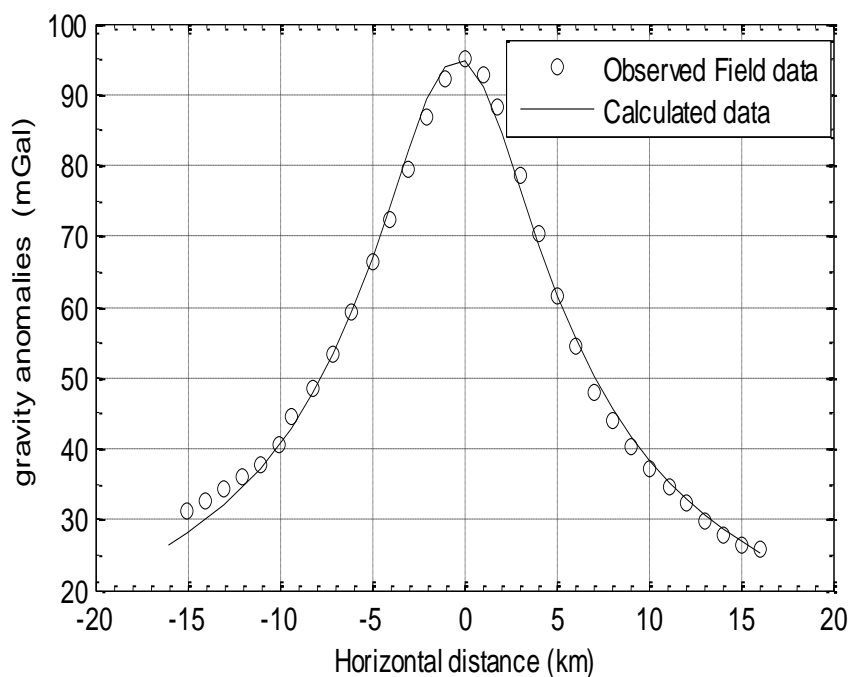


412  
413  
414  
415  
416  
417  
418  
419  
420  
421  
422  
423  
424  
425  
426  
427  
428  
429



430  
431  
432

Figure 6



433  
434  
435  
436  
437  
438  
439  
440  
441  
442  
443  
444  
445  
446  
447  
448



449 Table 1

Gravity data description	Weighting factor	$c_1 = 1.0,$ $c_2 = 1.0$	$c_1 = 1.2,$ $c_2 = 1.2$	$c_1 = 1.4,$ $c_2 = 1.4$	$c_1 = 1.6,$ $c_2 = 1.6$	$c_1 = 1.8,$ $c_2 = 1.8$	$c_1 = 2.0,$ $c_2 = 2.0$
		RMS Error					
Synthetic spherical body	$w = 0.4$	0.004899	0.002899	0.00014	0.000907	0.000853	0.000861
	$w = 0.7$	0.002532	0.000118	0.000013	0.000087	0.000187	0.000247
	$w = 0.9$	0.005215	0.000118	0.000063	0.000379	0.000167	0.002695
Synthetic vertical Cylindrical body	$w = 0.4$	0.004892	0.003231	0.000327	0.000835	0.000704	0.000932
	$w = 0.7$	0.001913	0.000318	0.000011	0.000065	0.000207	0.000511
	$w = 0.9$	0.003259	0.000551	0.000189	0.000183	0.001265	0.002747



450

451 Table 2

(a) Optimized Parameters, converged iteration and RMS error in the inversion of synthetic gravity anomaly over a spherical source model.						
Z (km)	A (mGal*km <sup>2</sup> )	q	g <sub>0</sub> (mGal)	x <sub>0</sub> (km)	Iteration	RMS Error (%)
4.99883	550	1.5	24.0	-1.89x10 <sup>-3</sup>	100	0.000405
4.9999	660.31	1.5	24.0	2.39x10 <sup>-5</sup>	200	0.000015
5.00	610.15	1.5	24.0	-1.44x10 <sup>-6</sup>	300	0.00
5.00	604.36	1.5	24.0	3.3x10 <sup>-13</sup>	400	0.00
5.00	604.10	1.5	24.0	8.17x10 <sup>-16</sup>	500	0.00
(b) Optimized Parameters, converged iteration and RMS error in the inversion of synthetic gravity anomaly with 10% white gaussian noise over a spherical source model.						
z (km)	A (mGal*km <sup>2</sup> )	q	g <sub>0</sub> (mGal)	x <sub>0</sub> (km)	Iteration	RMS Error (%)
4.5	605.49	1.5	24	-6.95X10 <sup>-2</sup>	100	0.174890
4.5	603.99	1.5	24	-6.81X10 <sup>-2</sup>	200	0.174885
4.5	550.32	1.5	24	-6.86X10 <sup>-2</sup>	300	0.174883
4.5	601.42	1.5	24	-6.86X10 <sup>-2</sup>	400	0.174883
4.5	680.0	1.5	24	-6.85X10 <sup>-2</sup>	500	0.174883

452

453

454

455

456



457

458 Table 3

(a) Optimized Parameters, converged iteration and RMS error in the inversion of synthetic gravity anomaly over a vertical cylindrical source model.						
Z (km)	A (mGal*km <sup>2</sup> )	q	g <sub>0</sub> (mGal)	x <sub>0</sub> (km)	Iteration	RMS Error (%)
3.015	182.31	0.5	66.33	-4.4x10 <sup>-3</sup>	100	0.001743
3.016	185.92	0.5	66.33	-3.7x10 <sup>-4</sup>	200	0.001635
3.016	192.59	0.5	66.33	-2.74x10 <sup>-10</sup>	300	0.001633
3.015	162.15	0.5	66.33	-7.98x10 <sup>-11</sup>	400	0.001633
3.016	169.00	0.5	66.33	-6.58x10 <sup>-11</sup>	500	0.001633
(b) Optimized Parameters, converged iteration and RMS error in the inversion of synthetic gravity anomaly with 10% white gaussian noise over a vertical cylindrical source model.						
z (km)	A (mGal*km <sup>2</sup> )	q	g <sub>0</sub> (mGal)	x <sub>0</sub> (km)	Iteration	RMS Error (%)
3.02	167.33	0.5	65.81	-3.95x10 <sup>-2</sup>	100	0.036732
2.99	160.38	0.5	66.33	1.36x10 <sup>-2</sup>	200	0.036968
3.02	161.74	0.5	65.88	-4.52x10 <sup>-2</sup>	300	0.036672
30.2	160.35	0.5	65.88	-4.50x10 <sup>-2</sup>	400	0.036672
3.02	198.67	0.5	65.88	-4.50x10 <sup>-2</sup>	500	0.036672

459

460

461

462

463



464

465 Table 4

(a) Optimized Parameters, converged iteration and RMS error in the inversion of field gravity anomaly over Mobrun sulphide ore body.						
z (km)	A (mGal*km <sup>2</sup> )	q	g <sub>0</sub> (mGal)	x <sub>0</sub> (km)	Iteration	RMS Error (%)
31	58.08	0.77	1.7781	-2.99078	100	0.027149
31	59.55	0.76	1.1156	-3.02429	200	0.027163
31	58.00	0.76	1.7826	-2.13091	300	0.027125
31	59.03	0.77	1.7826	-2.15033	400	0.027124
30	59.99	0.77	1.7992	-2.15013	500	0.027124
(b) Comparative results over Mobrun field example from various methods and GPSO.						
Parameter	Grant and West (1965)	Euler deconvoltuion (Roy et al., 2000)	Fast interpretation Method	Tuned- PSO Method		
Z(m)	30	29.44	33.3	30.0		
q	-	0.77	0.78	0.77		
A(mGal)	-	-	59.1	60.0		

466

467



468

469 Table 5

(a) Optimized Parameters, converged iteration and RMS error in the inversion of field gravity anomaly over West Senegal (Louga area) anomaly.						
z (km)	A (mGal*km <sup>2</sup> )	q	g <sub>0</sub> (mGal)	x <sub>0</sub> (km)	Iteration	RMS Error (%)
4.90	549.44	0.52	94.83	-2.60x10 <sup>-1</sup>	100	0.027065
4.90	550.0	0.53	94.80	-2.56x10 <sup>-1</sup>	200	0.026552
4.91	549.57	0.53	94.79	-2.45x10 <sup>-1</sup>	300	0.026552
4.91	547.66	0.53	94.79	-2.42x10 <sup>-1</sup>	400	0.026551
4.91	545.30	0.53	94.79	-2.39x10 <sup>-1</sup>	500	0.025551
(b) Comparative results of various methods over West Senegal (Louga area) anomaly.						
Parameter	New fast least square method (Essa, 2014)		Tuned-PSO method			
z (km)	4.94		4.92			
q	0.53		0.53			
A (mGal)	545.68		545.30			

470

471

472

473

474

475

476

477